ACS APPLIED MATERIALS & INTERFACES

Research Article

www.acsami.org

Facile Fabrication and Enhanced Photocatalytic Performance of Ag/AgCl/rGO Heterostructure Photocatalyst

Guoqiang Luo,[†] Xiaojuan Jiang,[†] Meijuan Li,[†,‡] Qiang Shen,[†] Lianmeng Zhang,*[,†] and Huogen Yu*[,‡]

[†]State Key Laboratory of Advanced Technology for Materials Synthesis and Processing, Wuhan University of Technology, Wuhan 430070, People's Republic of China

[‡]Department of Chemistry, School of Science, Wuhan University of Technology, Wuhan 430070, People's Republic of China

Supporting Information

ABSTRACT: Graphene/reduced graphene oxide (rGO) modification has been demonstrated to be an efficient route to improve the photocatalytic performance of various photocatalysts by promoting the effective separation of photogenerated electrons and holes. It is highly required to develop facile and environmental-friendly methods for the preparation of graphene-based photocatalytic materials. In this study, the Ag/AgCl/rGO heterostructure photocatalyst was fabricated by a mild oxidization reaction of hydrothermally prepared Ag/rGO in $FeCl_3$ solution. It was found that the reduction of graphene oxide (GO) was accompanied with the in situ formation of metallic Ag in a $Ag[(NH_3)_2]^+$-immobilized GO solution during hydrothermal treatment, while the following in situ oxidation of metallic Ag by $FeCl_3$ solution resulted in the formation of strongly coupled Ag/AgCl/rGO heterostructure photocatalyst. The photocatalytic experimental results indicated that all the resultant Ag/AgCl/rGO nanocomposite photocatalysts exhibited a much higher photocatalytic activity than the Ag/AgCl and physically mixed Ag/AgCl/rGO composite, and the Ag/AgCl/rGO (3.2 wt % rGO) showed the highest photocatalytic performance. The enhanced photocatalytic performance of Ag/AgCl/rGO heterostructures can be attributed to the cooperation effect of the effective separation of photogenerated carriers via strongly coupled rGO cocatalyst and the enrichment of organic molecules on the rGO nanosheets. Considering the facile preparation and its high photocatalytic activity, it is possible for the present Ag/AgCl/rGO nanocomposites to be widely applied in various fields such as air purification and wastewater treatment.

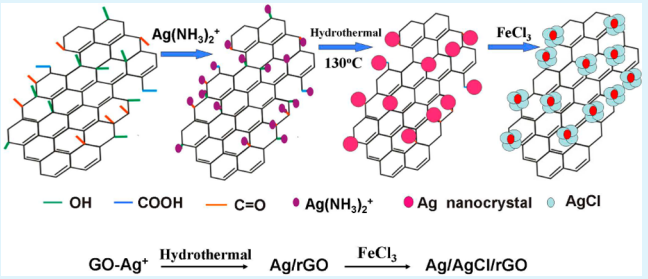

KEYWORDS: *graphene, Ag/AgCl, photocatalysis, heterostructure, interface*

1. INTRODUCTION

Development of highly efficient photocatalytic materials for the elimination of organic pollutants has been considered to be one of the important investigative fields.[1,2] TiO_2, a traditional photocatalyst, has been widely investigated because of its nontoxicity and long-term stability.[3−5] However, the TiO_2 photocatalyst still cannot be widely used in practical applications due to its limited visible-light absorption and low photocatalytic efficiency. Thus, it is highly required to develop new and efficient visible-light-responded photocatalysts. Recently, it was demonstrated that the silver halide (AgX, X = Cl, Br, I) could work as a new visible-light photocatalyst for the decomposition of various organic substances.[6−9] However, the silver halide photocatalysts should be further modified to enhance their photocatalytic performance from the viewpoint of potential applications. On the other hand, much attention has been paid to graphene due to its fascinating physical properties and potential various applications.[10,11] In the photocatalytic reactions, it is believed that graphene or reduced graphene oxide (rGO) can accelerate the separation process of photogenerated electrons and holes, resulting in a higher photocatalytic performance.[12−14] Considering the excellent electron mobility and large specific surface of the graphene, it is expected that the photocatalytic performance of silver halide photocatalysts can be further improved by the effective modification of graphene.

Recently, several groups have reported the synthesis of graphene-based silver halide photocatalysts.[15,16] Zhu et al. prepared the Ag/AgBr/graphene oxide (Ag/AgBr/GO) nanocomposite via an oil/water microemulsion method by a surfactant-assisted assembly protocol.[15] Zhang et al. also synthesized the graphene sheet grafted Ag@AgCl hybrid by a deposition−precipitation method to obtain AgCl/GO hybrids, which was followed by a photoreduction method to produce metallic Ag.[16] Owing to a high nucleation and growth rate of the AgBr or AgCl by the conventional aqueous solution route, the reported silver halide particles usually show a large size (≥500 nm) in the graphene-based photocatalysts.[15,16] Moreover, the severe aggregation of rGO is usually unavoidable due to its high hydrophobicity.[17,18] In addition, the present studies

Received: December 23, 2012
Accepted: February 21, 2013
Published: February 21, 2013

about the graphene-based photocatalytic materials are mainly focused on the reduction of GO, and seldom, researchers have paid attention to the enhanced coupling interaction between rGO nanosheets and the photocatalytic materials.[19−22] Considering the importance of charge transfer and separation in photocatalytic reactions, it is highly required to develop a new synthetic method for the preparation of Ag/AgX/rGO heterostructure with a strong coupling interface.

To develop highly efficient silver halide photocatalysts, it is very important to control the formation process of silver halides with a small particle size. Recently, Ye et al. and other researchers have developed an effective synthetic method for the preparation of silver halide particles via an in situ oxidation method of metallic Ag to silver halide by Fe^{3+} ions in the solution.[23−25] Compared with the rapid nucleation and growth rate of conventional precipitation reaction between Ag^+ and Cl^- (or Br^-), the in situ oxidation method of metallic Ag by Fe^{3+} ions is mild and can be easily controllable. In this study, the Ag/AgCl/rGO heterostructure photocatalyst was prepared by a hydrothermal treatment of $Ag[(NH_3)_2]^+$-immobilized GO solution and the following room-temperature in situ oxidation of Ag/rGO in a $FeCl_3$ solution. The effective reduction of GO to rGO and the formation process of the Ag/AgCl/rGO heterostructure were carefully characterized by various analysis methods, and the photocatalytic activities were evaluated by the photocatalytic decomposition of methyl orange (MO) and phenol solutions under visible-light irradiation. On the basis of the experimental results, a possible photocatalytic mechanism was proposed to account for the enhanced performance of the Ag/AgCl/rGO heterostructure photocatalysts. Considering the facile and environmental-friendly preparation route, it is possible for the highly efficient Ag/AgCl/rGO nanocomposites to be widely applied in various fields such as air purification and wastewater treatment.

2. EXPERIMENTAL SECTION

Materials. Graphite was provided from Nanjing XFNANO Materials Tech Co Ltd., and all the other reagents (analytical grade) were supplied by Shanghai Chemical Reagent Ltd. (P.R. China) and used as received without further purification.

Preparation of GO. The GO was synthesized from natural graphite powder (99.95%).[26] Briefly, 3 g of graphite, 2.5 g of $K_2S_2O_8$, and 2.5 g of P_2O_5 were added into 12 mL of concentrated H_2SO_4 under strong stirring at 80 °C for 4.5 h. After the solution was cooled down to room temperature naturally, 0.5 L of deionized (DI) water was added into the above solution and was then aged for 12 h. The suspension was filtered, washed, and dried to obtain the black solid. The black solid was mixed with 120 mL of concentrated H_2SO_4 and 15 g of $KMnO_4$ in an ice bath below 20 °C and was then transferred to a water bath and magnetically stirred at 35 °C for 2 h. The resultant dark-brown paste was diluted with the slow addition of 250 mL of DI water and then stirred for another 2 h; 20 mL (30 wt %) of H_2O_2 was slowly added to quench the solution to produce a golden-brown solution. After the product was centrifuged, the sample was washed with HCl (1:10) and DI water, respectively, until the pH of the washed solution was ca. 6. Finally, the product was dried at 40 °C in vacuum to obtain the GO sample. The GO aqueous solution (0.05 wt %) was prepared by ultrasonic dispersion of GO sample in DI water for 2 h to obtain a stable and homogeneous GO aqueous solution.

Preparation of Ag/rGO. Ag/rGO composite was synthesized by a one-step hydrothermal method using the GO and silver ammonia solution as the precursors. Silver ammonia solution was first prepared from 100 mL of $AgNO_3$ (0.1 M) and 10 mL of ammonia solution (3 M), and the GO solution was then added to the above silver ammonia solution to form a homogeneous mixing solution. After stirring for 10 min, the mixing solution was transferred to a Teflon-lined stainless steel autoclave (100 mL) and was then maintained at 130 °C for 3 h. After cooling down to room temperature, the resulting samples were filtered, washed, and dried at 60 °C for 5 h to obtain the Ag/rGO nanocomposite.

Preparation of Ag/AgCl/rGO. The Ag/AgCl/rGO nanocomposite was prepared by an in situ oxidation reaction between Ag/rGO and $FeCl_3$ aqueous solution in a dark condition. To prevent the rapid hydrolysis of Fe^{3+} ions, the pH of $FeCl_3$ solution (0.1 mol·L^{-1}) was adjusted to ca. 2.5 by using HCl solution (1 mol·L^{-1}). Typically, 0.5 g of the Ag/rGO nanocomposite was added to 80 mL of $FeCl_3$ solution under stirring at room temperature (25 °C). After stirring for some time (15−120 min), the product was filtered, washed with water, and dried at 60 °C for 5 h to obtain Ag/AgCl/rGO nanocomposites. To prepare the Ag/AgCl/rGO nanocomposites with a controllable component, the weight ratio of rGO to AgCl was controlled to be 0, 1.7, 2.3, 3.2, and 6.4 wt %, respectively, via adjusting the Ag^+ amount and GO solution. To simplify the sample name, the resulting product will be referred to as Ag/AgCl/rGO (X wt %), with X representing weight ratio of rGO to Ag.

For comparison, the Ag/AgCl photocatalyst was also prepared by a direct precipitation reaction shown as follows. Ten mL of $AgNO_3$ (0.05 M) and 10 mL of NaCl (0.05 M) solution was mixed under a dark condition to obtain AgCl powders. After rinsing with distilled water, the AgCl powder was put into a methyl orange (MO) solution and was then irradiated by a 350 W Xe lamp for 30 min to obtain Ag/AgCl photocatalyst.

Characterization. X-ray diffraction (XRD) patterns were obtained on a D/MAX-RBX-ray diffractometer (Rigaku, Japan). Morphological analysis was performed with an S-4800 field emission scanning electron microscope (FESEM) (Hitachi, Japan) with an acceleration voltage of 10 kV. Transmission electron microscope (TEM) analyses were conducted on a JEM-2100F electron microscope (JEOL, Japan) using a 200 KV accelerating voltage. Fourier Transform Infrared spectra (FTIR) were acquired using a Nexus FT-IR spectrophotometer (Thermo Nicolet, America). Raman spectra were collected using an INVIA spectrophotometer (Renishaw, UK). X-ray photoelectron spectroscopy (XPS) measurements were done on a KRATOA XSAM800 XPS system with Mg Kα source. All the binding energies were referenced to the C1s peak at 284.8 eV for the surface adventitious carbon.

Photocatalytic Activity. MO is a simple azo dye that has been widely used as a model system to probe the photocatalytic performance of various photocatalysts. It is generally considered to be very stable to light and difficult to be decomposed, though MO can absorb visible light at ca. 464 nm. The photocatalytic activity of the prepared samples was performed at ambient temperature.[27−29] Experimental details were shown as follows: 20 mg of the sample was dispersed into 10 mL of MO solution (20 mg/L) in a disk with a diameter of ca. 5 cm. The solution was allowed to reach an adsorption−desorption equilibrium among the photocatalyst, MO, and water before visible-light irradiation. A 350 W xenon lamp equipped with a UV-cutoff filter (providing visible light with $\lambda \geq 400$ nm) was used as a visible-light source. The average light intensity striking the surface of the reaction solution was about 40 mW·cm^2. The concentration of MO was determined by an UV−visible spectrophotometer (UV-1240, SHIMADZU, Japan). After visible-light irradiation for some time, the concentration of MO was measured. As for the methyl orange aqueous solution with low concentration, its photocatalytic decolorization is a pseudofirst-order reaction and its kinetics may be expressed as $\ln(c_0/c) = kt$, where k is the apparent rate constant and c_0 and c are the methyl orange concentrations at initial state and after irradiation for t min, respectively.[6,7] The adsorption performance of various photocatalysts for the MO was measured by using $(c_0-c_a)/c_0$, where the c_0 and c_a are the MO concentrations at initial state and after adsorption−desorption equilibrium, respectively.[12] In addition, the colorless phenol (10 mg L^{-1}) was also used as the target organic substance to evaluate the photocatalytic performance of Ag/AgCl/rGO composites under identical experimental conditions.[27,28]

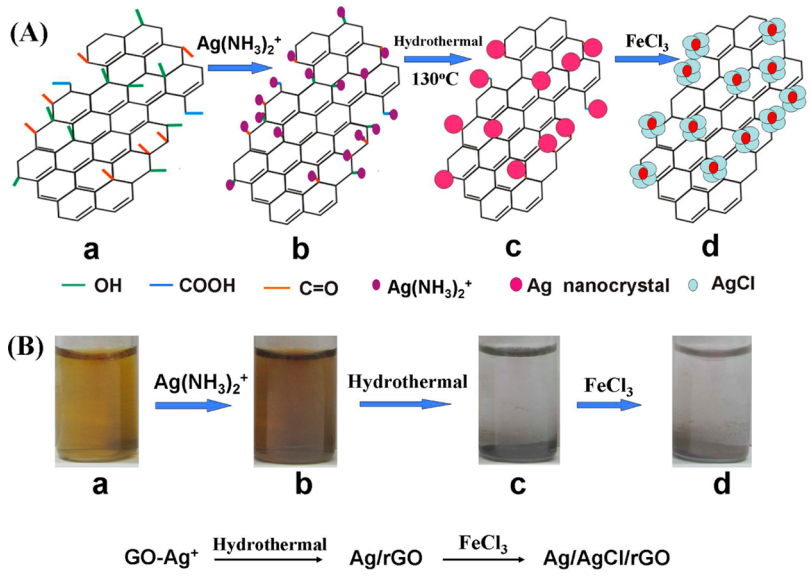

Figure 1. Schematic diagram illuminating the formation process of Ag/AgCl/rGO composite photocatalysts.

3. RESULTS AND DISCUSSION

Strategy for the Synthesis of Ag/AgCl/rGO Heterostructure. Figure 1A shows the schematic representation for the formation of Ag/AgCl/rGO composite photocatalyst. It is well-known that the chemically derived GO nanosheets can be well dispersed into water to form a homogeneous and stable solution (Figure 1B-a) owing to the abundant oxygen-containing functional groups such as hydroxyl, carbonyl, and carboxyl on their surface (Figure 1A-a).[30] When the GO solution was hydrothermally treated at 130 °C for 3 h, it was found that the brilliant yellow turned into black (Figure S1, Supporting Information), indicating the effective reduction of GO to rGO, in good agreement with the previous reports.[30] After the addition of silver ammonia solution into the above GO solution, its color changed into light brown (Figure 1B-b). The possible reason can be attributed to the electrostatic adsorption of positive $Ag[(NH_3)_2]^+$ ions on the surface of negative GO nanosheets (Figure 1A-b), which is beneficial to the following in situ formation of metallic Ag nanoparticles on the surface of GO nanosheets. When the $Ag[(NH_3)_2]^+$-immobilized GO solution was hydrothermally treated at 130 °C, a gray precipitate was formed on the bottom (Figure 1B-c), which can be ascribed to the Ag/rGO composite (see below). As a consequence, the effective reduction of GO nanosheets is accompanied with the formation of Ag nanoparticles from the $Ag[(NH_3)_2]^+$ ions during the hydrothermal process. Further observation indicates that, after the precipitation of the Ag/rGO composite, the resident solution is very clear and colorless (Figure 1B-c), which is completely different from the homogeneous and black rGO solution (Figure S1, Supporting Information) obtained from the pure GO solution after hydrothermal treatment. This can be attributed to the fact that the Ag nanoparticles can be well encapsulated by the rGO nanosheets (as shown in the SEM image), which is in favor of the following formation of Ag/AgCl/rGO heterostructure. Additional experimental results suggest that the rGO nanosheets can not be easily detached from the Ag nanoparticles by strong stirring or ultrasonic dispersion, suggesting that there is a strong interaction between the rGO nanosheets and Ag nanoparticles. When the strongly coupled Ag/rGO composite was oxidized by $FeCl_3$ aqueous solution at room temperature for 30 min, the gray color of Ag/rGO sample gradually turned lighter (Figure 1B-d) owing to the formation of white AgCl nanoparticles. Considering a higher redox potential of Fe^{3+}/Fe^{2+} (+0.771 V vs SHE) than the AgCl/Ag (+0.223 V vs SHE),[31] the metallic Ag on the rGO can be effectively oxidized by $FeCl_3$ to form AgCl under mild room-temperature conditions.[23−25] In addition, it is found that the resident solution is still very clear after the precipitation of Ag/AgCl/rGO composite, suggesting that the strong interaction between rGO nanosheets and the Ag nanoparticles can be well preserved after the in situ transformation of metallic Ag to AgCl. Therefore, the formation mechanism of the Ag/AgCl/rGO composites is based on the simultaneous reduction of GO and Ag^+ during hydrothermal treatment and the subsequent in situ oxidation of metallic Ag by $FeCl_3$ solution (Figure 1A).

It is found that both the GO and $Ag[(NH_3)_2]^+$ ions can be effectively reduced to rGO and metallic Ag nanoparticles, respectively, without the additional reducing agents. Therefore, compared with the well-known reduction of GO by hydrazine or sodium borohydride, in this study, there is an obviously different reduction mechanism. With increasing temperature and pressure, the physiochemical properties of water can be greatly changed, and the supercritical water becomes a fluid with unique properties such as strong electrolytic solvent power, high diffusion coefficient, and ion molecules.[32] In addition, it is believed that the high-temperature water can provide an effective environment to promote the cleavage reactions of various heterolytic bonds.[32] As a consequence, the hydrothermal method has been extensively used to prepare carbon-based nanostructures via the deoxygenation reaction of carbohydrates.[33,34] Therefore, the hydrothermal reduction mechanism of GO nanosheets can be attributed to the deoxygenation/dehydration reaction of GO, while the adsorbed $Ag[(NH_3)_2]^+$ ions can be in situ reduced by the carbonyl groups on the GO surface, resulting in their simultaneous reduction during the hydrothermal process.

Morphology and Microstructures of Ag/AgCl/rGO Heterostructure. The formation process of the Ag/AgCl/rGO heterostructure can be effectively demonstrated by the

dx.doi.org/10.1021/am303225n | ACS Appl. Mater. Interfaces 2013, 5, 2161−2168

XRD, FESEM, and TEM technologies. Figure 2 shows the XRD patterns of GO, rGO, Ag/rGO, and Ag/AgCl/rGO. The

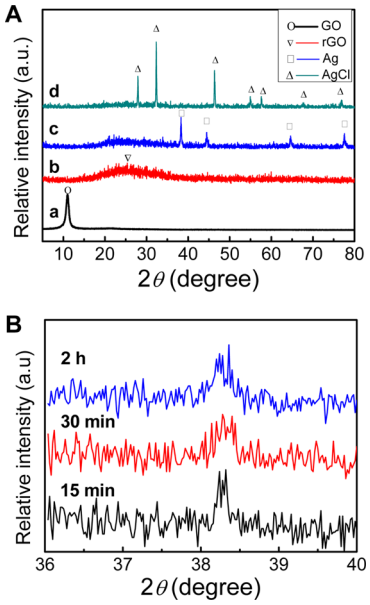

Figure 2. (A) XRD patterns of the (a) GO, (b) rGO, (c) Ag/rGO, and (d) Ag/AgCl/rGO (3.2 wt %); (B) The Ag diffraction peak of the Ag/AgCl/rGO (3.2 wt %) prepared from different oxidation time in $FeCl_3$ solution.

diffraction peak at 11.07° can be attributed to the characteristic peak of GO (Figure 2A-a).[35] After hydrothermal treatment of the GO solution, a new and broad diffraction peak at ca. 24° corresponding to rGO can be clearly observed while the characteristic peak of GO disappears completely (Figure 2A-b), indicating the effective reduction of GO to rGO, in good agreement with the previous studies.[12,35] The corresponding FESEM images of the GO (Figure 3a) and rGO (Figure S2, Supporting Information) show a similar smooth surface with a wrinkled structure, which is a typical characteristic of nanosheet-like structure. When the $Ag[(NH_3)_2]^+$-immobilized GO solution is hydrothermally treated, the characteristic peaks of metallic Ag can be clearly seen in addition to the rGO phase (Figure 2A-c), suggesting the successful formation of Ag/rGO composite. The Ag nanoparticles with a size of 10−200 nm are well encapsulated by the rGO nanosheets (Figure 3b,d), illustrating the well coupling between the rGO nanosheets and the Ag particles, in good agreement with the result in Figure 1. After the oxidation reaction of Ag/rGO in $FeCl_3$ aqueous solution, the characteristic peaks of rGO and AgCl (JCPDS no. 31-1238) can be clearly observed while the corresponding diffraction peaks of metallic Ag disappear completely (Figure 2A-d). To further demonstrate the metallic Ag, the characteristic diffraction peak at ca. 38.3° (JCPDS no. 41-1104) was measured and the corresponding results were shown in the Figure 2B. It is found that only a very weak diffraction peak of metallic Ag can be observed even after 15-min oxidation reaction, suggesting that the present oxidation method of Ag via $FeCl_3$ solution is a highly efficient strategy for the preparation of Ag/AgCl photocatalyst.[23−25] With further increase of the oxidation time to 2 h, however, the diffraction peak of metallic Ag can not disappear completely (Figure 2B), which can be attributed to the fact that the surface of metallic Ag is perfectly covered by the AgCl crystals and rGO nanosheets. Therefore,

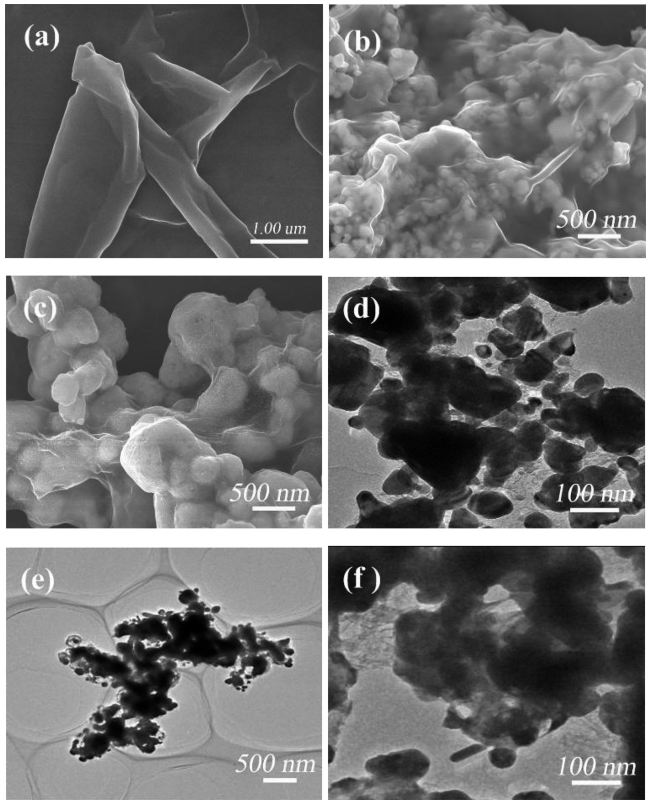

Figure 3. FESEM images of the (a) GO, (b) Ag/rGO, and (c) Ag/AgCl/rGO (3.2 wt %) and TEM images of the (d) Ag/rGO and (e,f) Ag/AgCl/rGO (3.2 wt %).

after reaction with $FeCl_3$ solution, the resultant sample can be attributed to the Ag/AgCl/rGO heterostructure composite. Considering an in situ oxidation process of metallic Ag on the rGO surface, the resultant Ag/AgCl/rGO composite (Figure 3c,e) also shows a well encapsulated structure similar to that of the Ag/rGO precursor (Figure 3b).

Compared with the reported Ag/AgCl/rGO composites,[15,16] one of the obvious advantages in this study is that the smaller AgCl particles (less than 400 nm) can be easily obtained in the final Ag/AgCl/rGO composite. In addition, the $Ag[(NH_3)_2]^+$ ions are first adsorbed on the active sites of GO nanosheets and are then in situ reduced to metallic Ag. In view of a homogeneous surface adsorption of $Ag[(NH_3)_2]^+$ ions on the GO nanosheets, it is clear that the resultant AgCl particles can be homogeneously coated on the rGO surface, as shown in the FESEM image (Figure 3b,c). Moreover, owing to an in situ formation of metallic Ag on the rGO nanosheets, it is believed that the strong coupling interface can greatly promote the rapid transfer of photogenerated electrons and improve the photocatalytic performance.

The effective reduction of GO to rGO and the formation process of Ag/AgCl/rGO can be further demonstrated by the FTIR, Raman, and XPS technologies. Figure 4 shows the FTIR spectra of GO, rGO, Ag/rGO, and Ag/AgCl/rGO samples. It is clear that the GO (Figure 4a) shows many strong absorption peaks that correspond to various oxygen functional groups, such as water −OH stretching (3410 cm^{-1}), carboxylates or ketones C═O stretching (1734 cm^{-1}), water −OH bending and C═C stretching (1629 cm^{-1}), alcoholic C−OH bending (1420 cm^{-1}), epoxide C−O−C or phenolic C−O−H stretching (1227 cm^{-1}), and C−O stretching (1055

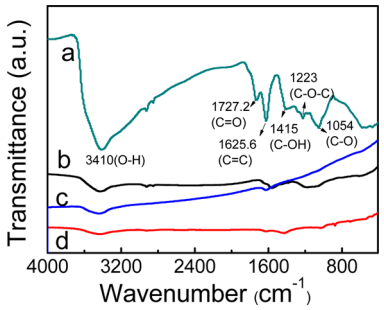

Figure 4. FTIR spectra of the (a) GO, (b) rGO, (c) Ag/rGO, and (d) Ag/AgCl/rGO (3.2 wt %).

cm^{-1}).[36,37] After hydrothermal treatment of the GO, the intensity of all absorption peaks corresponding to oxygen functional groups (C═O, C−OH, C−O−C, C−O−H, and C−O) has a significant decrease (Figure 4b), which further demonstrates the effective reduction of GO to rGO by the hydrothermal method, in good agreement with the XRD results (Figure 2). After the in situ loading of metallic Ag (Figure 4c) and AgCl (Figure 4d) particles on the rGO surface, both the resultant composites show a low absorption-peak intensity of the oxygen functional groups at 900−1800 cm^{-1}, similar to the rGO (Figure 4b). Therefore, the above results further confirmed the reduction of GO and the successful preparation of Ag/AgCl/rGO composites.

Raman spectroscopy is known as a powerful and widely used technique for the characterization of sp^2 and sp^3 hybridized carbon atoms in graphene to distinguish the order and disorder/defect structures.[37,38] The characteristic Raman peaks of GO, rGO, Ag/rGO, and Ag/AgCl/rGO samples are shown in the Figure 5. The G band (~1580 cm^{-1}) corresponds

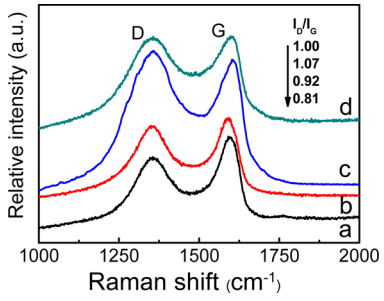

Figure 5. Raman spectra of the (a) GO, (b) rGO, (c) Ag/rGO, and (d) Ag/AgCl/rGO (3.2 wt %).

to the first-order scattering of the E_{2g} mode observed for sp^2 carbon domains, while the D band (~1350 cm^{-1}) is attributed to a breathing mode of κ-point phonons of A_{1g} symmetry, which is a common feature of sp^3 defects in carbon and usually can be associated with the structural defects, amorphous carbon, or edges that break the symmetry and selection rule.[38] As a consequence, the intensity ratio of the D band to the G band is usually a measure of the disorder/defects in graphene, and a smaller intensity ratio of I_D/I_G can be assigned to less sp^3 defects/disorders and larger average size (or less amount) of the in-plane graphitic crystallite sp^2 domains.[38,39] Compared with the GO (0.81), the rGO shows a higher I_D/I_G ratio (0.92), indicating that the rGO prepared from the hydrothermal method contains more defects. Considering a hydrothermal deoxygenation/reduction process, it is clear that the defects in the GO nanosheets cannot be well repaired by hydrothermal treatment and are still remaining after the removal of oxygen moieties. However, compared to the dramatically increased I_D/I_G ratio of the rGO prepared from the hydrazine monohydrate, the increased number of sp^3 defects caused by the hydrothermal method is still very limited.[32,39] For the Ag/rGO composites, the I_D/I_G ratio is further improved to 1.07, suggesting the formation of more sp^3 defects in carbon. The possible reason for the increased sp^3 defects can be attributed to the strongly coupled interaction between the metallic Ag nanoparticles and the rGO nanosheets. After in situ oxidation of the Ag/rGO by $FeCl_3$, the I_D/I_G ratio of the resultant Ag/AgCl/rGO has a slight decrease. However, it is clear that the Ag/AgCl/rGO composites still show a higher I_D/I_G ratio than the rGO nanosheets owing to the interaction between the AgCl and rGO, which is beneficial to the effective transfer and separation of photogenerated electrons and holes (shown below).

After the hydrothermal reaction of GO nanosheets and the formation of Ag/AgCl/rGO composites, the chemical state of carbon atoms in the hexagonal lattice of rGO was changed significantly owing to the deoxygenation reaction, which can be well illustrated by the XPS results (Figure 6). The C 1s XPS

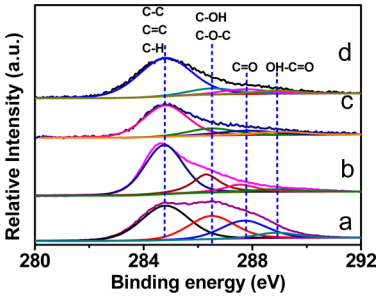

Figure 6. XPS spectra of C 1s in the (a) GO, (b) rGO, (c) Ag/rGO, and (d) Ag/AgCl/rGO (3.2 wt %).

spectrum of the GO nanosheets (Figure 6a) clearly shows the presence of four types of carbon bonds; that is, the nonoxygenated ring C (284.8 eV, including C−C, C═C, and C−H), the C−O in C−O−C or C−OH groups (286.5 eV), the carbonyl C in C═O (287.7 eV), and the carboxylate carbon in O═C−OH (288.9 eV), suggesting a considerable degree of oxidation for the GO nanosheets.[40] After hydrothermal treatment of the GO, the XPS peak intensity of these carbon−oxygen species in the resulting rGO (Figure 6b) shows a dramatic decrease, suggesting an effective deoxygenation of GO nanosheets. In view of an identical hydrothermal condition, it is clear that the GO in the $Ag[(NH_3)_2]^+$-immobilized GO solution can be effectively reduced to form rGO in the Ag/rGO (Figure 6c) and Ag/AgCl/rGO (Figure 6d) composites. To further illustrate the reduction degree of the GO nanosheets in the Ag/AgCl/rGO composite, the peak area ratios of oxygen-containing bonds to total area are calculated on the basis of XPS results and the corresponding results are shown in Table 1. It is clear that the amount of oxygen-containing groups such as C−OH, C−O−C, and C═O has a significant decrease, which further provides a strong evidence for the reduction of GO in Ag/AgCl/rGO composites. In addition, according to the XPS results, the metallic Ag on the surface of Ag/AgCl/rGO composite can be calculated to be 4.5 atom %.

dx.doi.org/10.1021/am303225n | ACS Appl. Mater. Interfaces 2013, 5, 2161−2168

Table 1. Composition (Atom %) of the Various Carbon Functional Groups According to the XPS Results

samples	C−C	C−O	C═O	COOH
GO	44.1	28.5	21.8	5.6
rGO	63.3	21.2	10.5	5.0
Ag/rGO	67.9	15.4	10.2	6.5
Ag/AgCl/rGO (3.2 wt %)	76.1	10.6	8.2	5.1

Photocatalytic Performance. The photocatalytic activities of the Ag/AgCl/rGO composites with a different amount of rGO were evaluated by the photocatalytic decomposition of MO solution, as shown in Figure 7. For comparison, the Ag/AgCl photocatalysts were also prepared and its photocatalytic performance was tested under an identical experimental condition. The controlled experimental results suggest that without photocatalysts the photobleaching of the MO in this study can be negligible. It is clear that the Ag/AgCl photocatalyst (Figure 7A-a) shows an obvious photocatalytic activity and the corresponding apparent rate constant (k) is 7.3 × 10^{-3} min^{-1} owing to its well-known visible-light photocatalytic performance. After the Ag/AgCl is coupled with rGO nanosheets, the resultant Ag/AgCl/rGO composites (Figure 7A-b,c) show a remarkable enhanced photocatalytic activity. Especially, when the amount of the rGO is controlled to be 3.2 wt %, the Ag/AgCl/rGO composite (Figure 7A-d) exhibits the highest photocatalytic activity with a k = 17.3 × 10^{-3} min^{-1}, a value larger than that of the Ag/AgCl by a factor of 2.4. With further increase of the rGO amount to 6.4 wt %, although the photocatalytic activity of the Ag/AgCl/rGO composite (Figure 7A-e) has a significant decrease (k = 12.1 × 10^{-3} min^{-1}), it still shows a higher photocatalytic performance than the Ag/AgCl photocatalyst. Apparently, graphene modification is an efficient route to improve the photocatalytic performance of Ag/AgCl photocatalysts. Further experimental results suggested that the prepared Ag/AgCl/rGO composite photocatalysts also exhibited effective photocatalytic decomposition for colorless phenol solution (Figure S3, Supporting Information).

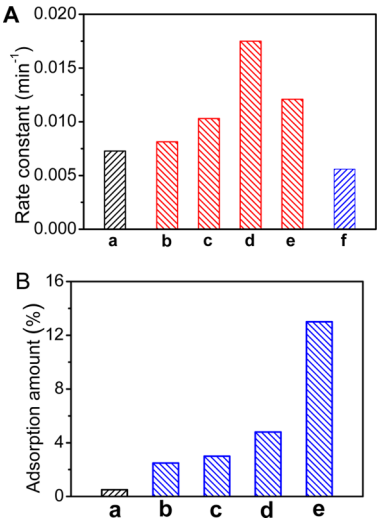

Figure 7. (A) Rate constant (k) of MO decomposition by various photocatalysts and (B) their corresponding adsorption ability: (a) Ag/AgCl, (b) Ag/AgCl/rGO (1.7 wt %), (c) Ag/AgCl/rGO (2.3 wt %), (d) Ag/AgCl/rGO (3.2 wt %), (e) Ag/AgCl/rGO (6.4 wt %), and (f) physically mixed Ag/AgCl/rGO (3.2 wt %).

For the enhanced photocatalytic performance of Ag/AgCl/rGO composite nanostructures, the effective coupling of Ag/AgCl particles on the rGO nanosheets is highly required. Additional experiments indicated that, when the Ag/AgCl particles were physically mixed with the rGO nanosheets, the resultant Ag/AgCl/rGO composite (Figure 7A-f) showed a lower photocatalytic performance than the Ag/AgCl particles (Figure 7A-a). In fact, it is found that the rGO can not be well coupled on the surface of Ag/AgCl particles and most of them are suspended on the surface of MO solution during photocatalytic testing. Therefore, the decreased photocatalytic performance of the physically mixed Ag/AgCl/rGO sample (Figure 7A-f) can be attributed to the increase in the opacity and light scattering of rGO, shielding the Ag/AgCl from absorbing visible light and resulting in rapid decrease of irradiation passing through the reaction solution.[41,42]

To investigate the enhanced photocatalytic mechanism of the Ag/AgCl/rGO composite, the adsorption ability of the Ag/AgCl/rGO composites for the MO solution was investigated, as shown in Figure 7B. It is clear that the adsorption ability for MO is greatly improved with increasing amount of rGO in the Ag/AgCl/rGO composite. Since the photocatalytic decomposition of organic substances takes place on the surface of a photocatalyst, the enrichment of the organic substances close to the photocatalysts is an important contributing factor for achieving higher photocatalytic performance.[41] In this study, MO molecules can diffuse to the surface of Ag/AgCl/rGO photocatalyst and be adsorbed on the rGO via $\pi-\pi$ conjugation between MO molecular and aromatic regions of graphene.[35,43]

Figure 8 shows the possible photocatalytic mechanism of the Ag/AgCl/rGO composites. It is well-known that the Ag/AgCl is an efficient visible-light photocatalyst. As AgCl cannot absorb visible light due to its wide band gap of 3.25 eV, the visible light absorption in Ag/AgCl can be attributed to the plasmonic absorption of metallic Ag nanoparticles. To investigate the photocatalytic mechanism of Ag/AgCl/rGO, it is important to know the band structure of AgCl phase. The CB energy level of AgCl can be calculated according to the equation of $E_c = -\chi + 0.5\ E_g$, where E_c, χ, and E_g are the CB energy level, absolute electronegativity and band gap of semiconductor, respectively.[44,45] Therefore, the CB and VB energy level of AgCl is calculated to be ca. −0.06 and 3.2 V (vs SHE), respectively. As the plasmon-induced electrons of metallic Au or Ag nanoparticles can transfer to the CB (−0.2 V, vs SHE) of anatase TiO_2 under visible-light irradiation,[46−48] it is believed that the plasmon-induced electrons of Ag nanoparticles with a strong reduction power can easily transfer to the CB (−0.06 V, vs SHE) of AgCl. Therefore, the possible photocatalytic

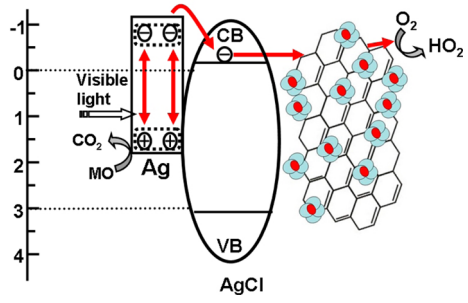

Figure 8. Schematic diagram illuminating the possible photocatalytic mechanism of Ag/AgCl/rGO composite photocatalysts.

mechanism of Ag/AgCl/rGO photocatalysts is that the plasmon-induced electrons of Ag nanoparticles transfer to the rGO nanosheets via the AgCl CB to reduce oxygen, while the plasmon-induced holes are retained on the surface of Ag nanoparticles to oxidize organic substances (Figure 8). Owing to the strong interaction between the interface of Ag/AgCl particles and the rGO nanosheets, the photogenerated electrons can be effectively transferred from AgCl to rGO surface. In this case, the rGO nanosheets work as a highly efficient cocatalyst for the rapid transfer of photogenerated electrons, resulting in a lower recombination rate and enhanced photocatalytic activity.[49] In fact, the rapid transfer mechanism of photogenerated electrons for the improved photocatalytic performance in this study is similar to the well-known noble metal-modified semiconductor photocatalysts, where the noble metal functions as an electron sink to accept photogenerated electrons from an excited semiconductor facilitating oxygen reduction.[50,51] In addition, the rGO nanosheets can also work as an effective platform for the enrichment of MO molecules, resulting in the improved photocatalytic performance (Figure 7B). First, the adsorbed MO molecules on the rGO surface can diffuse onto the active sites of Ag/AgCl photocatalyst for the further decomposition when the amount of adsorbed MO molecules is decreased with increasing irradiation time. Second, the active species such as ·OH and O_2^- can easily transfer to the surface of rGO to decompose the adsorbed MO molecules. Therefore, it is clear that the effective separation and high-efficiency utilization of photogenerated electrons and holes contribute to an obviously enhanced photocatalytic performance of the Ag/AgCl/rGO composite photocatalysts. In addition, it should be stressed that, compared with the expensive noble metal cocatalyst with a single function of promoting electron transfer, it is believed that the highly conductive graphene prepared from the large-scale produced GO precursor can be regarded as one of the ideal and novel cocatalysts to improve various semiconductor photocatalysts.

4. CONCLUSION

The Ag/AgCl/rGO heterostructure photocatalyst was successfully fabricated via a hydrothermal treatment of $Ag[(NH_3)_2]^+$-immobilized GO solution and the following room-temperature in situ oxidation of Ag/rGO by a $FeCl_3$ solution. It is found that the effective reduction of GO is accompanied with the in situ formation of metallic Ag on the rGO surface during hydrothermal reaction, while the following in situ oxidation of metallic Ag by $FeCl_3$ solution results in the formation of strongly coupled Ag/AgCl/rGO heterostructure photocatalyst. The photocatalytic experimental results indicate that all the resultant Ag/AgCl/rGO nanocomposite photocatalyst exhibits a much higher photocatalytic activity than the Ag/AgCl and physically mixed Ag/AgCl/rGO composite. Especially, the Ag/AgCl/rGO (3.2 wt % rGO) shows the highest photocatalytic performance. The enhanced photocatalytic performance of Ag/AgCl/rGO heterostructures can be attributed to the cooperation effect of the effective separation of photogenerated carriers via strongly coupled rGO cocatalyst and the enrichment of organic molecules on the rGO nanosheets. Considering the facile and environmental-friendly preparation route, it is possible for the highly efficient Ag/AgCl/rGO nanocomposites to be widely applied in various fields such air purification and wastewater treatment.

■ ASSOCIATED CONTENT

Supporting Information

The photograph of the rGO solution obtained from the hydrothermally treated GO solution, FESEM image of rGO nanosheets, and the rate constant of phenol decomposition. This material is available free of charge via the Internet at http://pubs.acs.org.

■ AUTHOR INFORMATION

Corresponding Author

*E-mail: lmzhang@whut.edu.cn (L.Z.); yuhuogen@yahoo.cn (H.Y.).

Notes

The authors declare no competing financial interest.

■ ACKNOWLEDGMENTS

This work was supported by the National Natural Science Foundation of China (21277017, 61274129, 51208396, and 51202175), 973 Program (2013CB632402), 863 Program (2012AA062701), and the 111 Project (B13035).

■ REFERENCES

(1) Kumar, S. G.; Devi, L. G. *J. Phys. Chem. A* **2011**, *115*, 13211.
(2) Zhao, Z. G.; Miyauchi, M. *Angew. Chem., Int. Ed.* **2008**, *47*, 7051.
(3) Yu, H. G.; Irie, H.; Shimodaira, Y.; Hosogi, Y.; Kuroda, Y.; Miyauchi, M.; Hashimoto, K. *J. Phys. Chem. C* **2010**, *114*, 16481.
(4) Yu, H. G.; Irie, H.; Hashimoto, K. *J. Am. Chem. Soc.* **2010**, *132*, 6898.
(5) Qiu, X. Q.; Miyauchi, M.; Sunada, K.; Minoshima, M.; Liu, M.; Lu, Y.; Li, D.; Shimodaira, Y.; Hosogi, Y.; Kuroda, Y.; Hashimoto, K. *ACS Nano* **2012**, *6*, 1609.
(6) Wang, X. F.; Li, S. F.; Yu, H. G.; Yu, J. G. *J. Mol. Catal. A: Chem.* **2011**, *334*, 52.
(7) Wang, X. F.; Li, S. F.; Ma, Y. Q.; Yu, H. G.; Yu, J. G. *J. Phys. Chem. C* **2011**, *115*, 14648.
(8) Wang, P.; Huang, B. B.; Qin, X. Y.; Zhang, X. Y.; Dai, Y.; Wei, J. Y.; Whangbo, M. H. *Angew. Chem., Int. Ed.* **2008**, *47*, 7931.
(9) Wang, P.; Huang, B. B.; Zhang, X. Y.; Qin, X. Y.; Jin, H.; Dai, Y.; Wang, Z. Y.; Wei, J. Y.; Zhan, J.; Wang, S. Y.; Wang, J. P.; Whangbo, M. H. *Chem.—Eur. J.* **2009**, *15*, 1821.
(10) Singh, V.; Joung, D.; Zhai, L.; Das, S.; Khondaker, S. I.; Seal, S. *Prog. Mater. Sci.* **2011**, *56*, 1178.
(11) Xiang, Q. J.; Yu, J. G.; Jaroniec, M. *Chem. Soc. Rev.* **2012**, *41*, 782.
(12) Wang, P.; Wang, J.; Wang, X. F.; Yu, H. G.; Yu, J. G.; Lei, M.; Wang, Y. G. *Appl. Catal., B: Environ.* **2013**, *132*−*133*, 452.
(13) Shah, M.; Park, A. R.; Zhang, K.; Park, J. H.; Yoo, P. J. *ACS Appl. Mater. Interfaces* **2012**, *4*, 3893.
(14) Zhu, P. N.; Nair, A. S.; Peng, S. J.; Yang, S. Y.; Ramakrishna, S. *ACS Appl. Mater. Interfaces* **2012**, *4*, 581.
(15) Zhu, M.; Chen, P.; Liu, M. *Langmuir* **2012**, *28*, 3385.
(16) Quan, X.; Zhang, H.; Fan, X. F.; Chen, S.; Yu, H. T. *Environ. Sci. Technol.* **2011**, *45*, 5731.
(17) Stankovich, S.; Piner, R. D.; Chen, X. Q.; Wu, N. Q.; Nguyen, S. T.; Ruoff, R. S. *J. Mater. Chem.* **2006**, *16*, 155.
(18) Gao, W.; Alemany, L. B.; Ci, L. J.; Ajayan, P. M. *Nat. Chem.* **2009**, *1*, 403.
(19) Liu, J.; Bai, H.; Wang, Y.; Liu, Z.; Zhang, X.; Sun, D. D. *Adv. Funct. Mater.* **2010**, *20*, 4175.
(20) Zhang, X. Y.; Li, H. P.; Cui, X. L.; Lin, Y. H. *J. Mater. Chem.* **2010**, *20*, 2801.
(21) Sher Shah, M. S. A.; Park, A. R.; Zhang, K.; Park, J. H.; Yoo, P. J. *ACS Appl. Mater. Interfaces* **2012**, *4*, 3893.
(22) Lambert, T. N.; Chavez, C. A.; Hernandez-Sanchez, B.; Lu, P.; Bell, N. S.; Ambrosini, A.; Friedman, T.; Boyle, T. J.; Wheeler, D. R.; Huber, D. L. *J. Phys. Chem. C* **2009**, *113*, 19812.

(23) Bi, Y. P.; Ye, J. H. *Chem. Commun.* **2009**, 6551.
(24) Bi, Y. P.; Ye, J. H. *Chem.—Eur. J.* **2010**, *16*, 10327.
(25) Xu, Y. G.; Xu, H.; Li, H. M.; Yan, J.; Xia, J. X.; Yin, S.; Zhang, Q. *Colloids Surf., A* **2013**, *416*, 80.
(26) Xu, Y.; Bai, H.; Lu, G.; Li, C.; Shi, G. *J. Am. Chem. Soc.* **2008**, *130*, 5856.
(27) Yu, H. G.; Liu, R.; Wang, X. F.; Wang, P.; Yu, J. G. *Appl. Catal., B: Environ.* **2012**, *111*, 326.
(28) Yu, H. G.; Liu, L.; Wang, X. F.; Wang, P.; Yu, J. G.; Wang, Y. H. *Dalton Trans.* **2012**, *41*, 10405.
(29) Wang, X. F.; Li, S. F.; Yu, H. G.; Yu, J. G.; Liu, S. W. *Chem.—Eur. J.* **2011**, *17*, 7777.
(30) Williams, G.; Seger, B.; Kamat, P. V. *ACS Nano* **2008**, *2*, 1487.
(31) Bard, A. J.; Parsons, R.; Jordan, J. *Standard Potentials in Aqueous Solution*; Marcel Dekker: New York, 1985.
(32) Zhou, Y.; Bao, Q.; Tang, L. A. L.; Zhong, Y.; Loh, K. P. *Chem. Mater.* **2009**, *21*, 2950.
(33) Sun, X. M.; Li, Y. D. *Angew. Chem., Int. Ed.* **2004**, *43*, 597.
(34) Yao, C.; Shin, Y.; Wang, L.-Q.; Windisch, C. F.; Samuels, W. D.; Arey, B. W.; Wang, C.; Risen, W. M.; Exarhos, G. J. *J. Phys. Chem. C* **2007**, *111*, 15141.
(35) Perera, S. D.; Mariano, R. G.; Vu, K.; Nour, N.; Seitz, O.; Chabal, Y.; Balkus, K. J. *ACS Catal.* **2012**, *2*, 949.
(36) Li, Q.; Guo, B. D.; Yu, J. G.; Ran, J. R.; Zhang, B. H.; Yan, H. J.; Gong, J. R. *J. Am. Chem. Soc.* **2011**, *133*, 10878.
(37) Shen, J.; Li, T.; Long, Y.; Shi, M.; Li, N.; Ye, M. *Carbon* **2012**, *50*, 2134.
(38) Luo, D. C.; Zhang, G. X.; Liu, J. F.; Sun, X. M. *J. Phys. Chem. C* **2011**, *115*, 11327.
(39) Wang, H. L.; Robinson, J. T.; Li, X. L.; Dai, H. J. *J. Am. Chem. Soc.* **2009**, *131*, 9910.
(40) Akhavan, O.; Abdolahad, M.; Esfandiar, A.; Mohatashamifar, M. *J. Phys. Chem. C* **2010**, *114*, 12955.
(41) Zhang, Y.; Tang, Z.-R.; Fu, X.; Xu, Y.-J. *ACS Nano* **2010**, *4*, 7303.
(42) Wang, F.; Zhang, K. *J. Mol. Catal. A: Chem.* **2011**, *345*, 101.
(43) Zhang, H.; Lv, X.; Li, Y.; Wang, Y.; Li, J. *ACS Nano* **2009**, *4*, 380.
(44) Xu, Y.; Schoonen, M. A. A. *Am. Mineral.* **2000**, *85*, 543.
(45) Scaife, D. E. *Sol. Energy* **1980**, *25*, 41.
(46) Tian, Y.; Tatsuma, T. *J. Am. Chem. Soc.* **2005**, *127*, 7632.
(47) Xiang, Q. J.; Yu, J. G.; Cheng, B.; Ong, H. C. *Chem. Asian J.* **2010**, *5*, 1466.
(48) Wu, T. S.; Wang, K. X.; Li, G. D.; Sun, S. Y.; Sun, J.; Chen, J. S. *ACS Appl. Mater. Interfaces* **2010**, *2*, 544.
(49) Wang, W. G.; Yu, J. G.; Xiang, Q. J.; Cheng, B. *Appl. Catal., B: Environ.* **2012**, *119*, 109.
(50) Liu, R.; Wang, P.; Wang, X. F.; Yu, H. G.; Yu, J. G. *J. Phys. Chem. C* **2012**, *116*, 17721.
(51) Yu, J. G.; Xiong, J. F.; Cheng, B.; Liu, S. W. *Appl. Catal., B: Environ.* **2005**, *60*, 211.